A model based approach to understanding the phase locking of ENSO and the annual cycle

This unpublished manuscript is the result of a term project conducted by Kristopher B. Karnauskas and Lisa N. Murphy while in the graduate program of the Department of Atmospheric and Oceanic Sciences at the University of Maryland–College Park. Original date: December 12, 2005.

Abstract

The present study is an investigation into the physical underpinnings of the phase locking between ENSO and the annual cycle. An appreciable amount of work has been aimed at this and similar questions, particularly observational studies resulting from the TOGA decade. In contrast, relatively little modeling efforts have been directed at understanding why peak conditions of most El Niño events in recent decades have occurred in boreal winter. Current knowledge of the global effects of El Niño remains based on observations of El Niño impacting the Earth during boreal winter. Using an OGCM of the tropical Pacific Ocean and various in situ data, it is found that the first order explanation of the seasonal timing of ENSO events, simply that westerly wind bursts occur during that season, is far short of complete. Rather, the state of the ocean is itself better situated thermodynamically to respond to the wind anomalies that are believed to play an important role in the genesis of El Niño events.

1. Introduction

Throughout the past 50 years, observations have shown Westerly wind bursts (WWBs) in the western Pacific before the onset of each El Niño. However, a wind stress anomaly is not a sufficient condition for an El Niño. The question of why the surface manifestations of El Niño most often occur in boreal winter remains unresolved. WWBs remain a primary research interest because of their perceived role in forcing oceanic changes that result in SST anomalies of more than 0.5°C (Harrison et al., 1997). The degree of warming is similar to what is observed during the onset of El Niño (Vecchi et al., 2000). Additionally, the subsurface thermal structure responds to warm, downwelling Kelvin waves that are excited by WWBs.

Studies have shown the onset of the 1997-98 El Niño was related to several WWBs in the western and central Pacific, although this is not necessarily true of every El Niño. A WWB in 1986, which led to a SSTA of 1°C in the eastern equatorial Pacific, was shown to have an insignificant effect on the subsequent 1986-87 El Niño (McPhaden et al., 1988). Furthermore, westerly wind event activity was particularly strong in January of 1993, yet it did not lead to El Niño conditions (Vecchi et al., 2000). Various mechanisms have been thought to generate WWBs, such as the existence of tropical cyclones on either side of the equator, cross equatorial flow, and the Madden-Julian Oscillation (MJO) (Harrison et al., 1997). A study by Eisenman et al. (2005) has shown that WWBs are three times more common when the western Pacific warm pool extends past the date line. Observational and modeling evidence further suggests that WWBs are the "tail" of ENSO, not the "dog," to use the analogy provided in Eisenman et al. (2005). Eisenman et al. (2005) concluded that WWBs are both stochastic forcing for ENSO and

are themselves affected by large-scale ENSO dynamics. While it was concluded that WWBs are modulated by ENSO, Eisenman et al. (2005) does not suggest that WWBs play an important role in ENSO forcing. Although El Niño conditions are generally thought to peak in a preferential season, model results have shown that the phase locking behavior is not this simple and can actually be scattered about the preferred season. It has been suggested that the phase locked nature of ENSO owes itself to nonlinear interactions, including atmospheric stochastic noise, between ENSO variability and the annual cycle (Neelin et al., 2000).

One could hypothesize that the forcing of the coupled system toward El Niño conditions occurs most often in boreal winter, or alternatively, that the system is prime to respond to the forcing in boreal winter. Analysis of satellite-derived pseudostress data from the Florida State University shows that WWBs in fact occur all year, with the most events occurring in the month of August (Fig. 1). For the same wind stress anomaly, the ocean might have a significantly different response which could depend on the state of the ocean or coupled system at that time. Insight into why El Niño peaks in winter can allow the community to examine possibility that this wasn't always the case, and how it may change in the future. Current knowledge of the global effects of El Niño is based on observations of El Niño impacting the Earth during boreal winter. The effects that ENSO events might have on climate if such events were to occur during the opposite time of the year are unknown and will remain so as long as boreal winter El Niños remain the norm. However, until sufficient explanation is offered for why boreal winter El Niños are the norm, the community must embrace the possibility that the future could hold summer El Niños, of which we have little basis for understanding.

Understanding and predicting ENSO was a major objective for Tropical Ocean Global Atmosphere (TOGA), however, numerical models were still unable to predict the 1997-98 ENSO event more than one season in advance (Barnston et al., 1999). Our knowledge of the dynamics and ocean-atmosphere coupling of the tropical Pacific Ocean and its season and interannual variability is still limited (also see Neelin et al., 1998). The Tropical Ocean-Global Atmosphere program of the 1980s had the objective of studying climate variability through the coupled ocean-atmosphere system. TOGA facilitated in the development of coupled models by implementing the Tropical Atmosphere Ocean (TAO; Soreide, 2004) moored buoys that can provide in situ datasets needed to validate models (McPhaden, 1998).

The objective of the present study is to better understand the physical processes underpinning the phase locking of El Niño conditions with the annual cycle. The hypotheses that will be tested include: El Niño conditions occur in boreal winter because (1) boreal winter is when westerly wind bursts occur, (2) WWBs only produce Kelvin waves in boreal winter, (3) the ocean is primed to respond to WWBs in boreal winter, (4) the coupled ocean-atmosphere system is primed to respond to westerly wind bursts in boreal winter, and (5) there is an hypothetical upper limit to SST such that an SST anomaly in boreal summer would result in SST exceeding the hypothetical upper limit.

2. Data and methods

Ocean general circulation modeling together with the analyses of in situ observations of SST, surface winds, and other relevant fields are employed to determine if there are any characteristics of the ocean, or the system in general, that is

preconditioned to better respond to the forcing for El Niño in boreal winter. A reduced-gravity, primitive equation, sigma co-ordinate model (Gent and Cane, 1989) of the tropical oceans, which is currently in at the Earth System Science Interdisciplinary Center of the University of Maryland and other leading research centers such as the NASA/Goddard Laboratory for Hydrospheric Processes, the National Center for Atmospheric Research, and the Lamont-Doherty Earth Observatory, will be used in the present study. Murtugudde et al. (1996) coupled the Gent-Cane OGCM to a simple atmospheric mixed layer model. It has been shown that the inclusion of the AML leads to significant improvements in simulated tropical SSTs. Recent advancements to the code allow realistic simulations for irregular coastline geometry, an option for vertical mixing schemes, and a choice of heat flux parameterizations (Gent and Cane, 1989). The model structure explicitly resolves the variable depth oceanic mixed layer (Chen et al., 1994) and the thermocline, the interactions between which can be better represented with enhanced resolution below the mixed layer. The model has been used extensively in ocean studies and even applied to ocean-ecosystem interactions (Wang et al., 2005).

Surface wind speed from the NCEP-NCAR reanalysis facilitated in determining the approximate area and magnitude of WWBs that have occurred during the most recent significant El Niño events (Fig. 2). This region was found to span the area of 130°E-170°E, 4°S-10°N. Initial conditions for the Gent-Cane OGCM were provided by the Atlas of Levitus et al. (1994). An initial model spin up was performed using climatological European Center for Medium-Range Weather Forecasts (ECMWF) winds until a stable seasonal cycle has developed. Four two-year simulations were produced during which small (0.02 Nm^{-2} or 4.3 ms^{-1}) and large (0.08 Nm^{-2} or 8.5 ms^{-1}) westerly

wind stress anomalies were superimposed upon the climatological winds. The wind stress anomalies were applied to the same region as was found to be appropriate based on analysis of observed zonal wind speed anomalies (Fig. 3). A small and a large westerly wind stress anomaly was applied during both the boreal summer (April-July) and boreal winter (October-January).

For the purposes of the present and other studies, a consistent and tractable dataset utilizing all available TAO measurements was produced. This dataset takes advantage of measurements of surface wind, air temperature, relative humidity, SST, and subsurface temperatures for the upper 500 meters of the water column. These data were used to validate various model-based claims in the present study.

3. Results and discussion

All four of the simulated El Niño events are reasonably similar to El Niño events observed in nature, both in spatial structure and temporal evolution. Shown in Figure 4 are time-longitude diagrams of the evolution of SST anomaly across the equatorial Pacific Ocean for each of the four simulated El Niños. The large winter and large summer El Niños were characterized by sustained SST anomalies of roughly 3°C in the eastern Pacific Ocean. Likewise, the small winter and small summer El Niños were characterized by sustained SST anomalies of roughly 1.5°C in the eastern Pacific. The large El Niños better represented the evolution of SST anomaly in the western Pacific Ocean with an accompanying negative anomaly. A comparison of the surface manifestation of the simulated large winter El Niño in January with the observed structure of the 1997-1998 El Niño in January is provided in Figure 5. Again, the El

Niños simulated in the present study are thought to be well suited for investigating the annual phase locking of ENSO events.

A closer examination of the evolution of each of the four simulated El Niños, using SST anomaly in the NIÑO3 region as the primary index (5°S–5°N x 150°W–90°W), reveals important differences between the summer and winter simulations. Figure 6 shows the evolution of SST anomaly in the NIÑO3 region throughout the four simulated El Niños. The bottom panel is simply the same as the top with the exception that all four time series have been shifted so that t=0 on the abscissa corresponds with the first time that the westerly wind stress anomaly was applied. In this manner, the magnitudes, duration, onset, and termination of each of the four simulated El Niños may be compared directly. Surprisingly, both of the summer El Niños were of greater magnitude than their corresponding winter El Niño. The NIÑO3 SST anomaly of the large summer El Niño, at its peak, was 0.5°C greater than that of the large winter El Niño. However, the onsets of both of the summer El Niños were slightly delayed relative to the onsets of the winter El Niños.

Since each of the simulated El Niños were induced by applying an anomaly to the climatological ocean state for some time in the year, a look at the seasonal evolution of the control run heat budget is necessary. From the OGCM, each of the ocean mixed layer heat budget components are calculated (Fig. 7). The dominant seasonal balance appears to be shortwave radiation balanced by longwave and latent heat fluxes. During the boreal fall (the sun's second annual crossing of the equator), entrainment mixing becomes one of the dominant factors balancing the shortwave flux. Figure 8 is the same as Figure 7, with the exception that only the heat budget components that consistently tend to cool the

mixed layer of the ocean are displayed, and the full two years of the control run are shown to facilitate seasonal comparisons. The only term that is particularly disparate between summer and winter is latent heat flux. Latent heat flux is also the most dominant mixed layer-cooling term, and is the least prohibitive of mixed layer warming in the winter- when El Niños peak in nature. During the summer, latent heat flux is the strongest (cooling the mixed layer the most) and would tend to be most prohibitive of mixed layer warming during that season.

Recall from the bottom panel of Figure 6 that the summer El Niños, while stronger, were slightly delayed toward winter. It could thus be proposed that the summertime response to a westerly wind stress anomaly is delayed because the ocean is not yet in the state least prohibitive of mixed layer warming. Provided in Figure 9 is the anomalous heat budget terms for the large summer and large winter El Niños. It can be seen that the anomalous latent heat flux for the summer El Niño is greater than that of the large winter El Niño, as is the case for nearly all heat budget terms.

The equatorial thermocline from the control simulation during summer and winter is shown in Figure 10. The equatorial thermocline in the east, where warm SST anomalies associated with El Niño events manifest themselves, is shallower in summer than in winter, thus the first order conclusion would be that El Niño conditions would tend more to peak in the summer. However, comparison of the structure of the basin-wide equatorial thermocline between summer and winter reveals an interesting fact. The structure of the basin-wide equatorial thermocline more resembles that during El Niño conditions in the winter, and during the summer, the basin-wide equatorial thermocline more resembles the thermocline during normal conditions. This is corroborated in Figure

11 with surface and subsurface temperature measurements from the TAO array of moorings. Figures 12 and 13 are depth sections of temperature anomaly (modeled and observed) for winter minus summer and during El Niño, respectively. This comparison highlights the fact that the winter state of the Pacific Ocean more resembles El Niño than does the summer state.

To summarize, many facets of the world dictate that El Niño conditions should peak in boreal summer (e.g. westerly wind stress anomalies peak in August, the eastern Pacific thermocline is shallower in the summer, and the simulated boreal summer El Niños were stronger than the simulated boreal winter El Niños in response to the same anomalous forcing). However, two characteristics of the boreal winter Pacific Ocean, which are evidently very important characteristics, dictate accurately that El Niños should peak in winter. As long as the Pacific Ocean is such that (1) the equatorial thermocline is flatter in boreal winter (more El Niño-like) than in the summer, (2) latent heat flux cools the mixed layer the most in boreal summer, and (3) extreme summertime westerly wind bursts do not dominate the seasonal cycle of winds, El Niños will continue to peak in boreal winter. The present study featured an OGCM coupled thermodynamically to the atmospheric mixed layer. Future studies should employ models in which the ocean and atmosphere are both thermodynamically and dynamically coupled.

References

Barnston, A. G., M. H. Glantz, and Y. He, 1999: Predictive skill of statistical and dynamical climate models in SST forecasts during the1997-98 El Niño episode and the 1998 La Niña onset. *Bull. Amer. Meteor. Soc.*, 80, 217-243.

Chen, D, L.M. Rothstein, and A.J. Busalacchi, 1994: A hybrid vertical mixing scheme and its application to tropical ocean models, *J. Phys. Oceanogr.*, 24, 2156-79.

Eisenman, I, Yu, L, and E. Tziperman: 2005: Westerly Wind Bursts: ENSO's tail rather than the dog?, *J. of Climate*.

Gent, P.R., and M.A. Cane, 1989: A Reduced Gravity, Primitive Equation Model of the Upper Equatorial Ocean. Journal Comput. Phys., 81, 444-480.

Kalnay, E. and Coauthors, 1996: The NCEP/NCAR Reanalysis 40-year Project. BAMS, 77, 437-471.

Harrison, D. E., and G. A. Vecchi, 1997: Westerly Wind Events in the Tropical Pacific, 1986-95, *J. of Climate*, 10, 12, 3131-3156.

Levitus and T. Boyer, 1994: World Ocean Atlas 1994 Vol. 4: Temp. NOAA Atlas NESDIS 4.

McPhaden, M. J., A. J. Busalacchi, R. Cheney, J. R. Donguy, K. S. Gage, D. Halpern, M. Ji, P. Julian, G Meyers, G. T. Mitchum, P. P. Niiler, J. Picaut, R. W. Reynolds, N. Smith, and K. Takeuchi, 1998: The Tropical Ocean-Global Atmosphere observing system: A decade of progress. *J. of Geophys. Res.*, 103, C7.

_____, H. P. Freitag, S. P. Hayes, B. A. Taft, Z. Chen, and K. Wyrtki, 1988: The response of the equatorial Pacific Ocean to a westerly wind burst in May 1986, *J. of Geophys. Res.*, 97, 14, 289-14 303.

Murtugudde, R., R. Seager, and A. Busalacchi, 1996: Simulation of the Tropical Oceans with an Ocean GCM Coupled to an Atmospheric Mixed-Layer Model, *J. Climate*, 9, 1795-1815.

Neelin, J. D., D. S. Battisti, A. C. Hirst, F. –F. Jin, Y. Wakata, T. Yamagata, and S. Zebiak, 1998: ENSO Theory, *J. Geophys. Res.*, 103, C7, 14261-14290.

Neelin, J. D., F. Jin, and H. Syu, 2000: Variations in ENSO Phase Locking, *J. of Climate*, 13, 2570-2590.

Soreide, N. N., L. C. McCarty, and D. C. McClurg, 1994: The Second International World Wide Web Conference '94: Mosaic and the Web, Chicago, Oct. 17-20, 1994. (Oral presentation). URL: http://www.pmel.noaa.gov/toga-tao/www94paper.html.

Vecchi, G. A., and D. E. Harrison, 2000: Tropical Pacific Sea Surface Temperature Anomalies, El Niño, and Equatorial Westerly Wind Events, *J. of Climate*, 13, 11, 1814-1830.

Wang X., R. Murtugudde, A. J. Busalacchi, and R. Le Borgne 2005. De-coupling of net community production and new production in the euphotic zone of the equatorial Pacific: A model study. *Geophysical Research Letters*, *32*, doi:10.1029/2005GL024100.

Figure 1. Climatology of significant westerly wind stress anomalies ($>10m^2s^{-2}$) in the domain (4°S-10°N x 130°E-170°E) over the period 1978-2003. Data: FSU pseudostress.
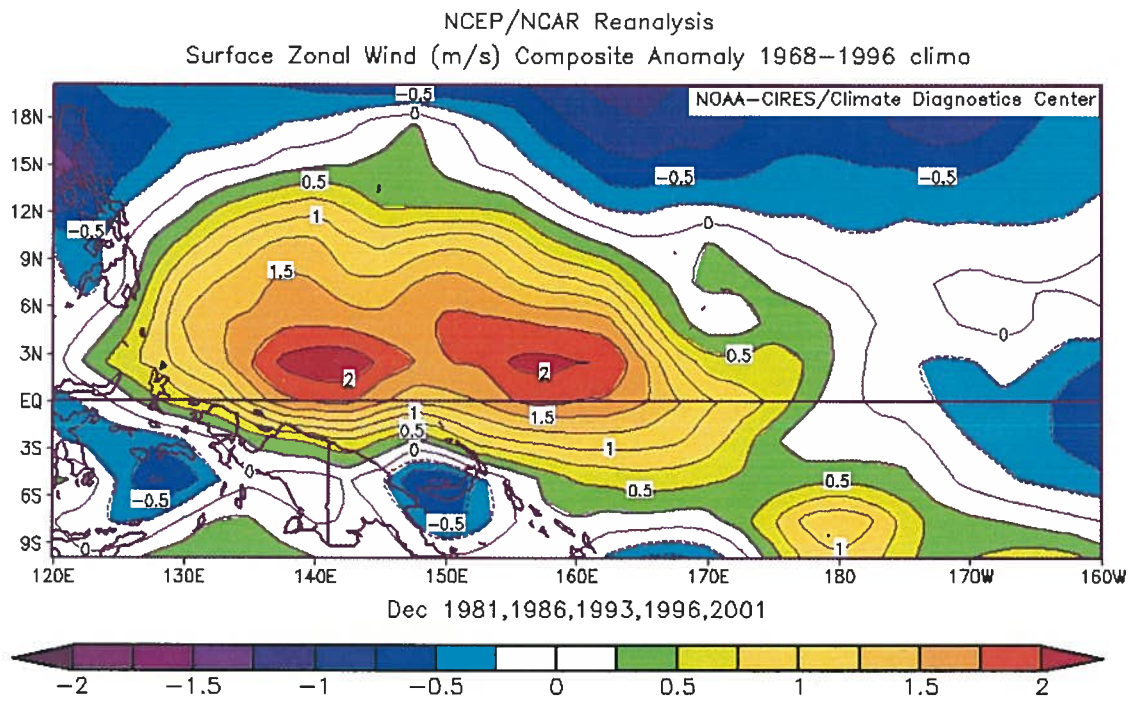

Figure 2. Composite surface zonal wind speed anomaly for the years shown above.
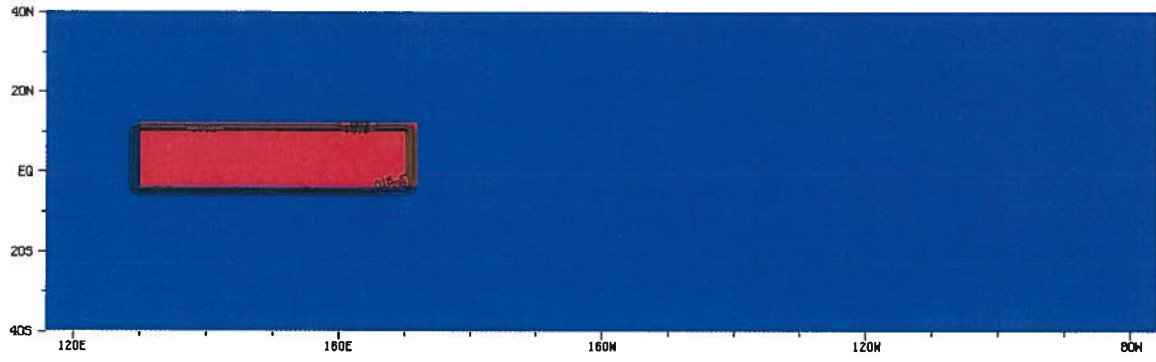

Figure 3. Zonal wind stress anomaly added to the climatological zonal wind stress for the times described in the Data and Methods section.
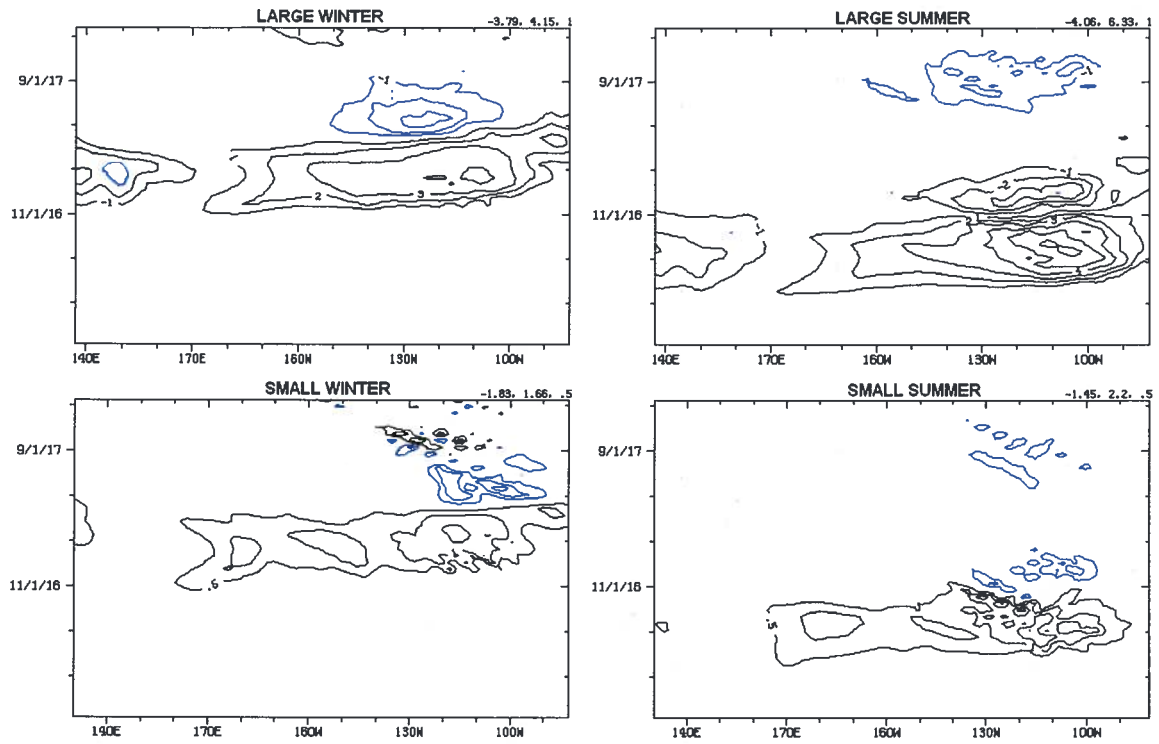

Figure 4. Time-longitude plots of SST anomalies along the equator for the four simulated El Niños.

Figure 5. Top: SST anomaly for January of simulated large winter El Niño. Bottom: Same as top but for the 1997-1998 El Niño (TAO dataset).

Figure 6. Top: Time series of SST anomaly in the NIÑO3 region for the four simulated El Niños. Red lines are summer and blue lines are winter. Bottom: Same as top but all time series are shifted so that t=0 on the abscissa corresponds to the time at which the westerly wind stress anomaly was imposed.

Figure 7. All ocean mixed layer heat budget components from one year of the control simulation.

Figure 8. Same as Figure 7 but for only the negative heat budget terms.

Figure 9. Evolution of heat budget component anomalies for the large summer simulation (top) and large winter simulation (bottom).

Figure 10. Simulated depth section of temperature along the equator for July (top) and January (bottom). The heavy line indicates the 20°C isotherm and represents the thermocline.

Figure 11. Observed depth section of temperature along the equator for July (top) and January (bottom). The heavy line indicates the 20°C isotherm and represents the thermocline.

Figure 12. Simulated depth section of temperature *difference* between January minus July along the equator for control simulation (top) and observations (bottom).

Figure 13. Simulated depth section of temperature anomaly along the equator during the peak El Niño conditions of the large winter simulation (left) and that observed in December 1988 from the TAO array (right).

Figure 1. Climatology of significant westerly wind stress anomalies ($>10\mathrm{m}^2\mathrm{s}^{-2}$) in the domain (4°S-10°N x 130°E-170°E) over the period 1978-2003. The abscissa is month of year, and the ordinate is number of events. Data: FSU pseudostress.

Figure 2. Composite surface zonal wind speed anomaly for the years shown above.

Figure 3. Zonal wind stress anomaly added to the climatological zonal wind stress for the times described in the Data and Methods section.

Figure 4. Time-longitude plots of SST anomalies along the equator for the four simulated El Niños described in Section 2.
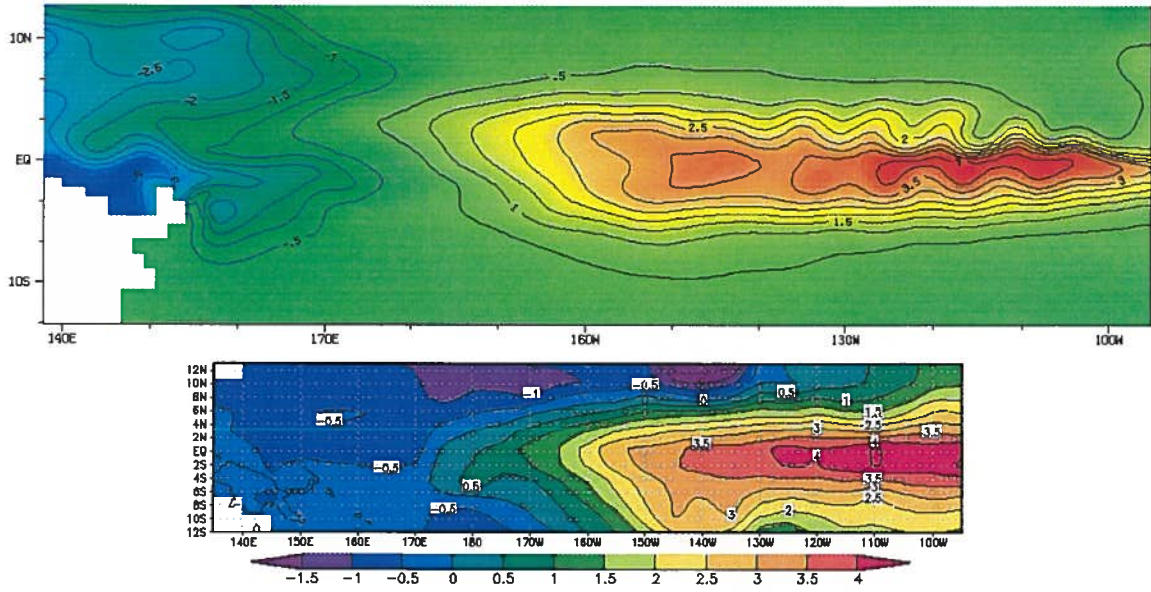
Figure 5. Top: SST anomaly for January of simulated large winter El Niño. Bottom: Same as top but for the 1997-1998 El Niño (TAO dataset).
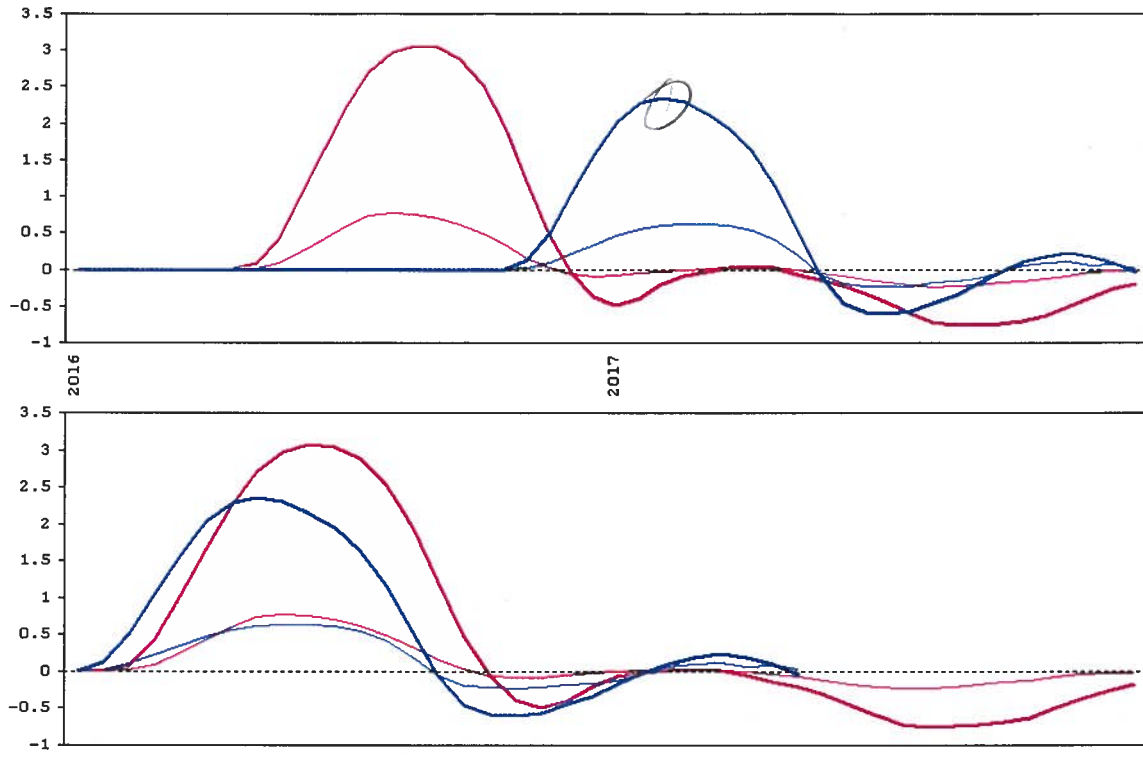
Figure 6. Top: Time series of SST anomaly (°C) in the NIÑO3 region for the four simulated El Niños. Red lines are summer and blue lines are winter. Bottom: Same as top but all time series are shifted so that t=0 on the abscissa corresponds to the time at which the westerly wind stress anomaly was imposed.
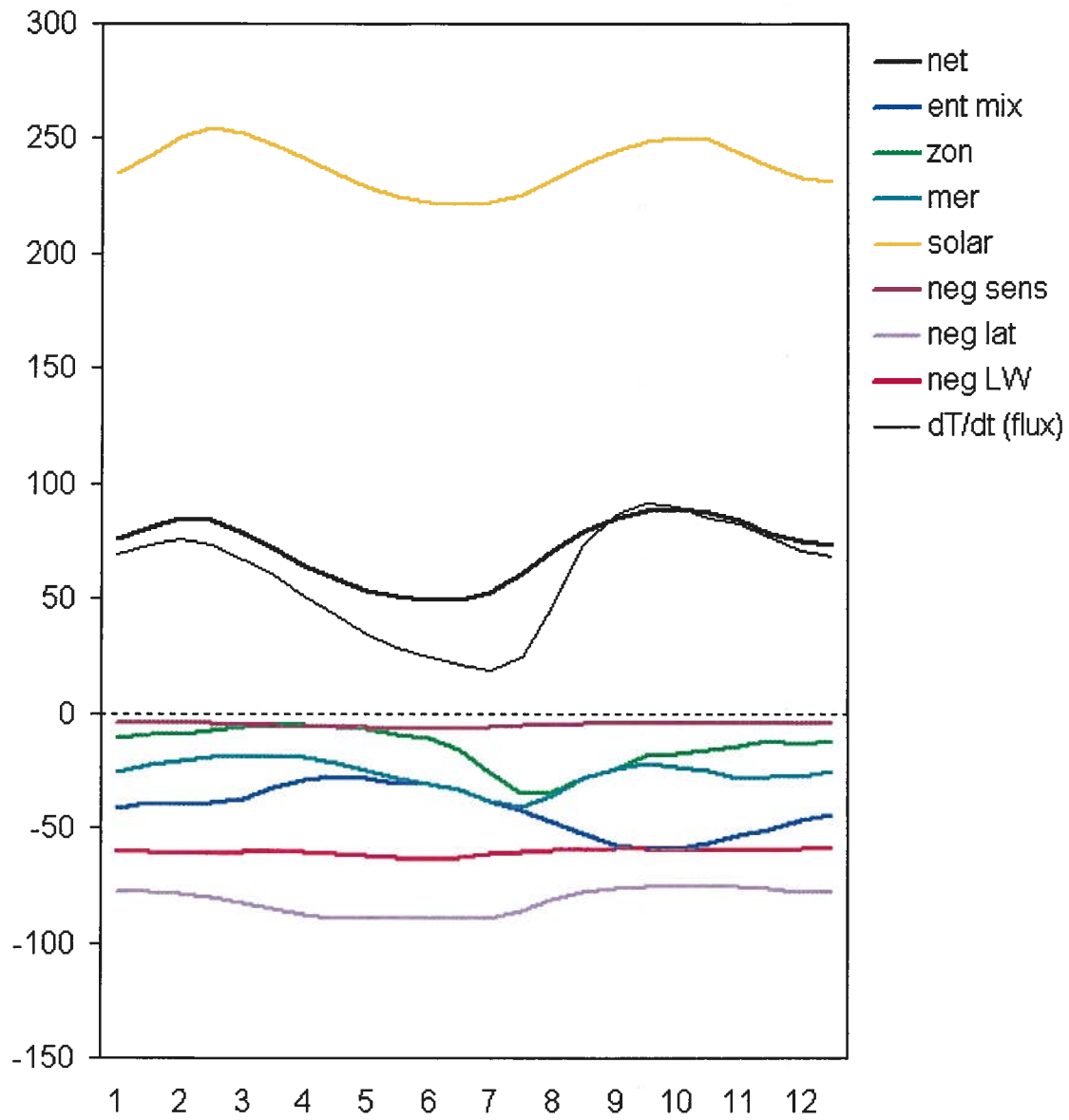
Figure 7. All ocean mixed layer heat budget components from one year of the control simulation. The abscissa is month of year, and the ordinate is energy flux (Wm^{-2}).
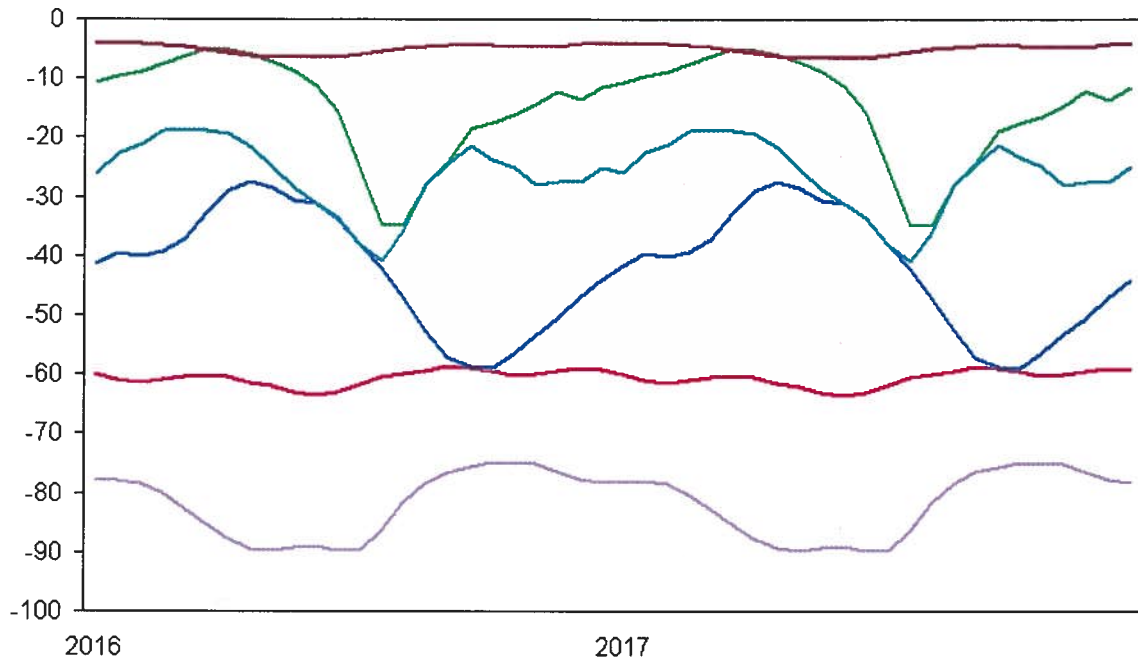
Figure 8. Same as Figure 7 but for the negative (mixed layer-cooling) heat budget terms only.
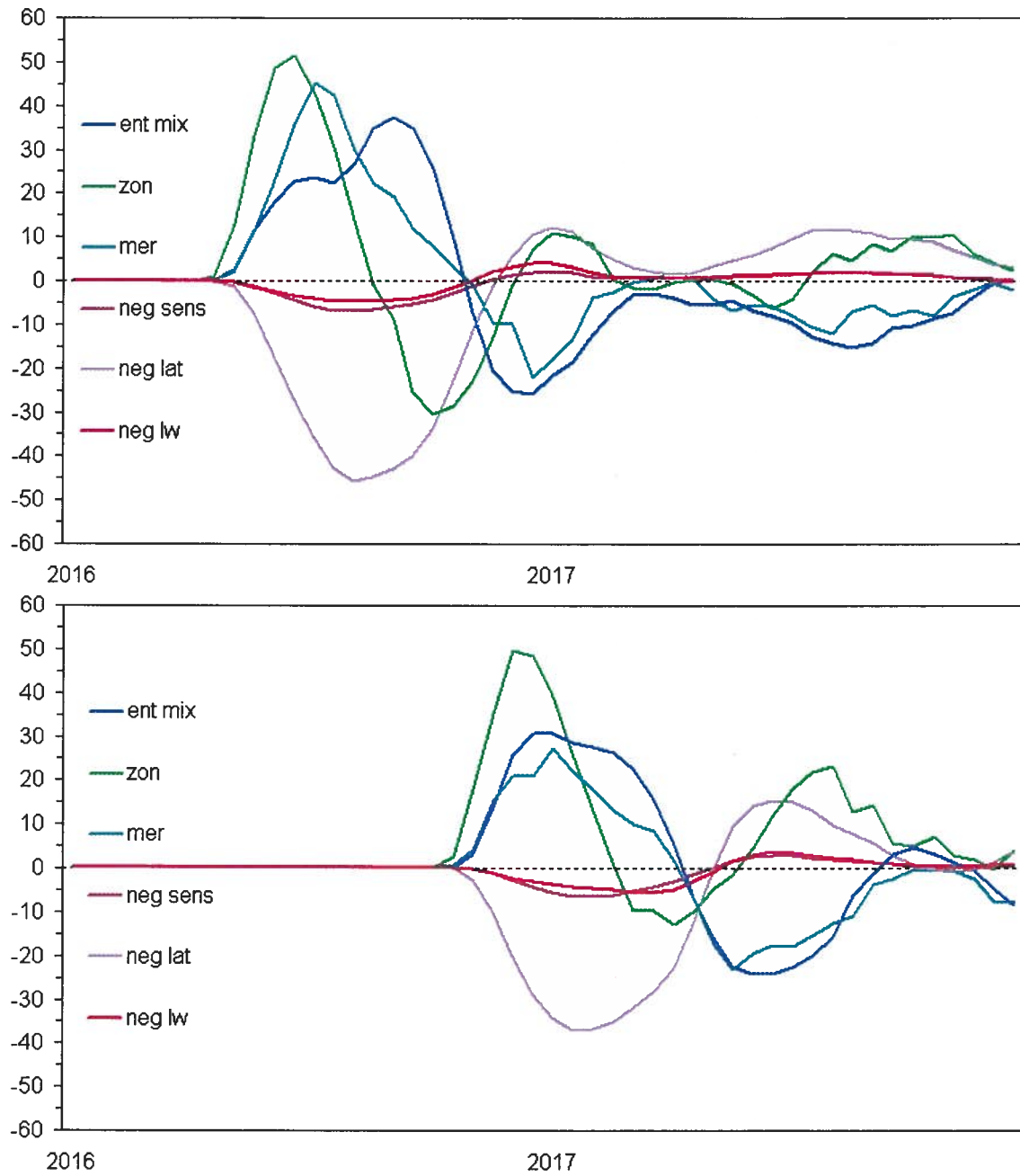
Figure 9. Evolution of heat budget component anomalies for the large summer simulation (top) and large winter simulation (bottom). The abscissa is time and includes the full two years of either simulation.
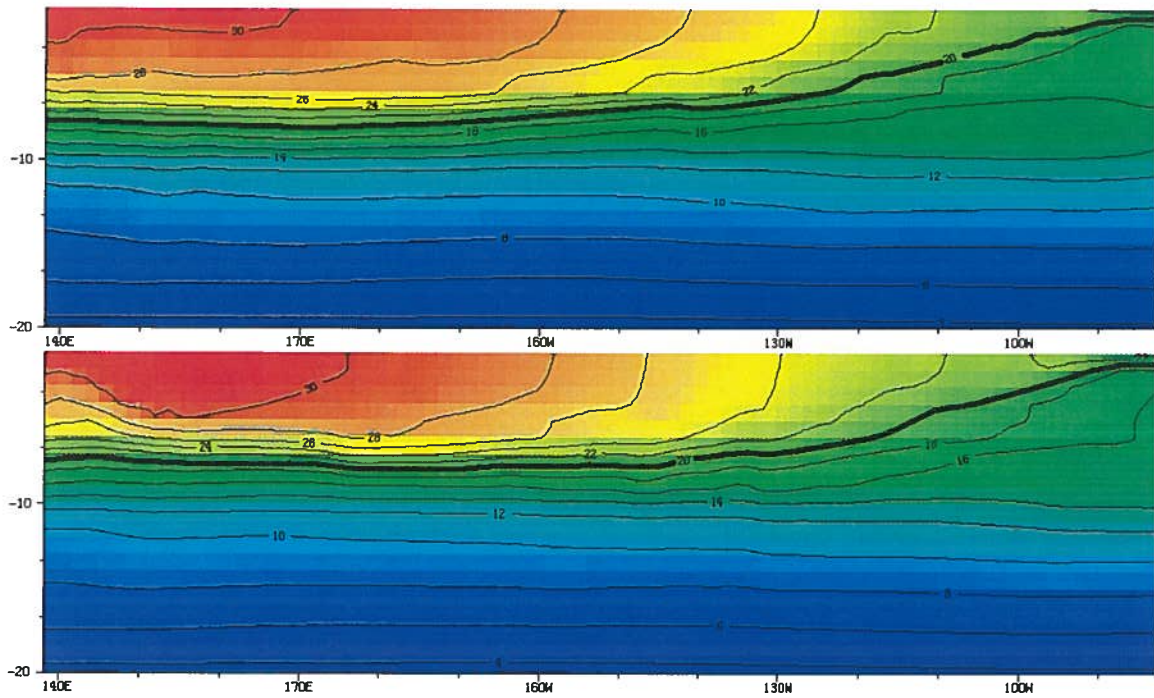
Figure 10. Depth sections of temperature along the equator for July (top) and January (bottom) from the control simulation. The heavy line indicates the 20°C isotherm and represents the thermocline.
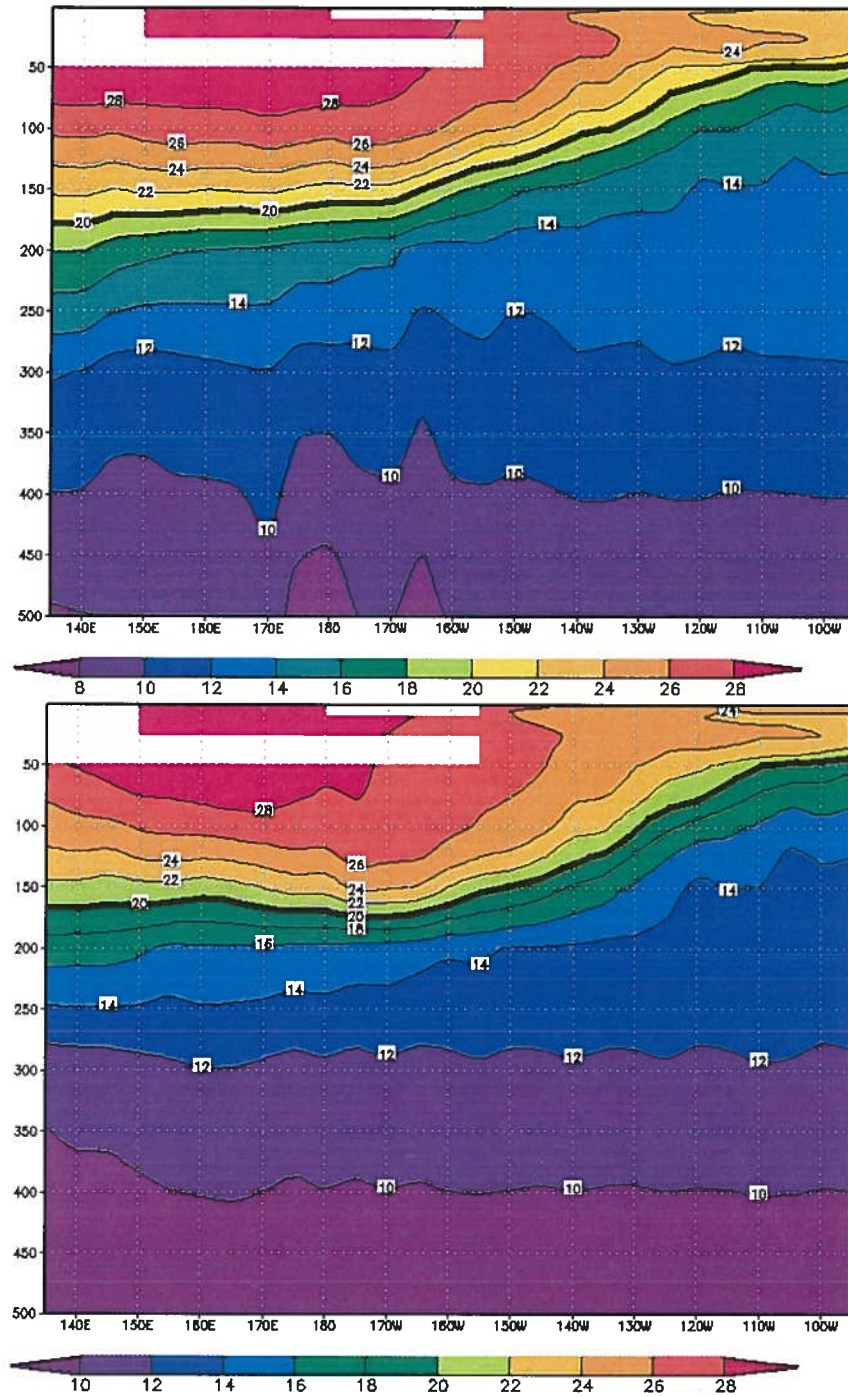
Figure 11. Observed depth sections of temperature along the equator for July (top) and January (bottom). The heavy line indicates the 20°C isotherm and represents the thermocline.
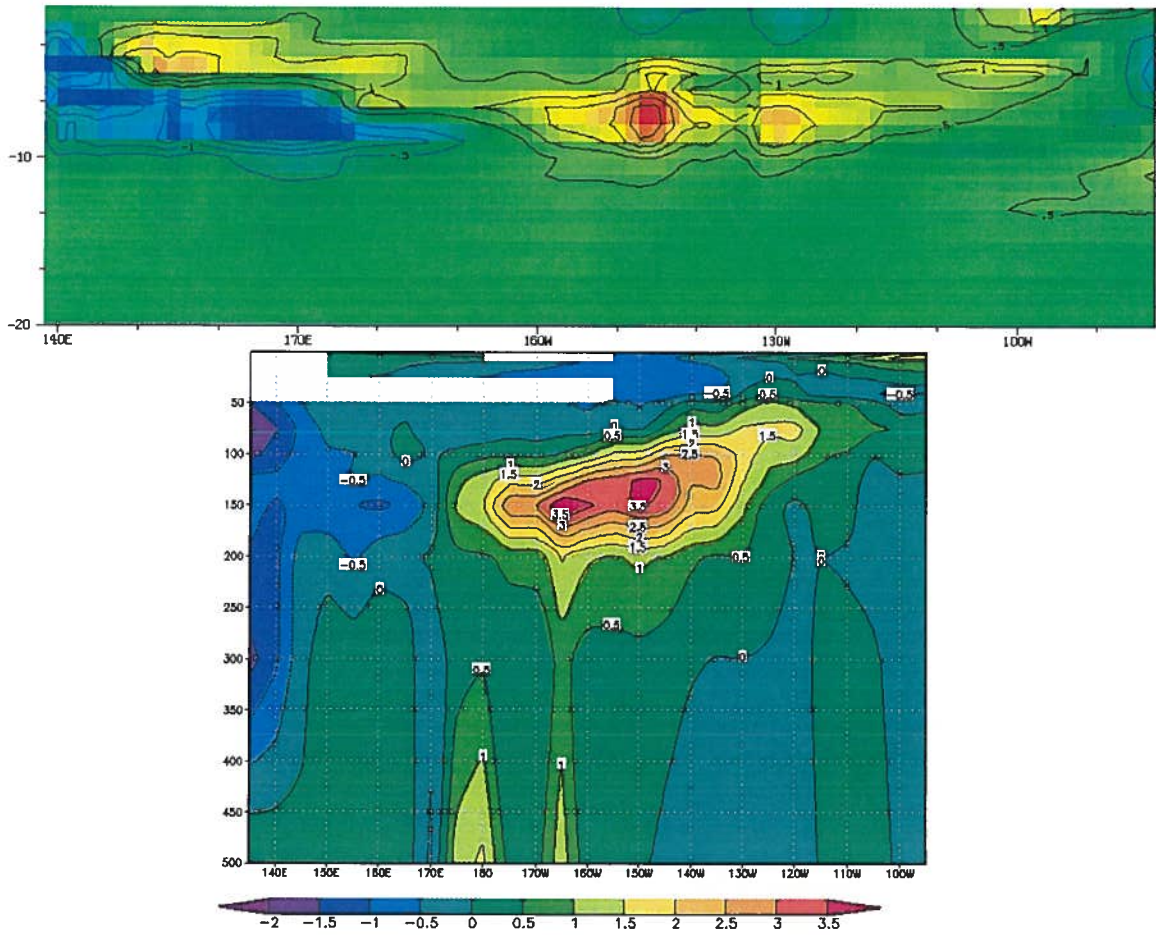
Figure 12. Simulated depth section of temperature *difference* between January minus July along the equator for control simulation (top) and observations (bottom).
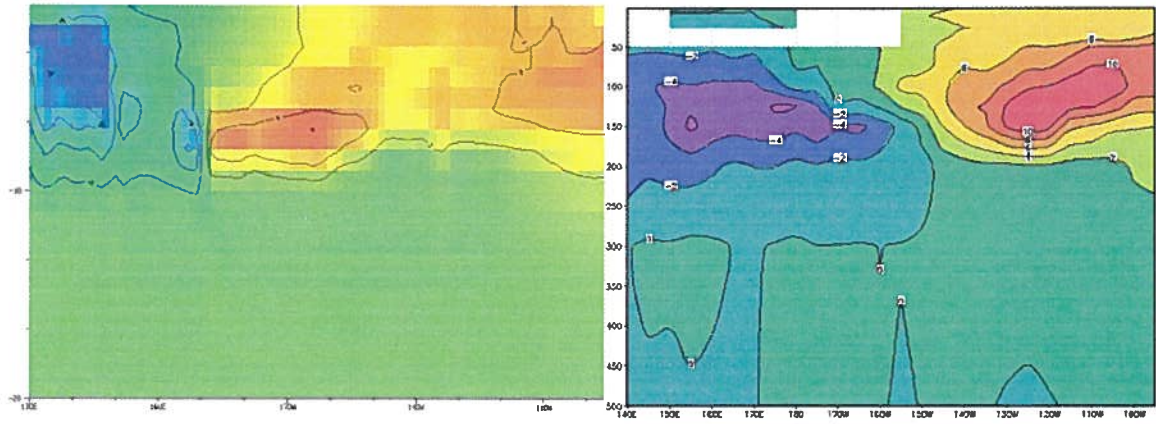
Figure 13. Simulated depth section of temperature anomaly along the equator during the peak El Niño conditions of the large winter simulation (left) and that observed in December 1988 from the TAO array (right).